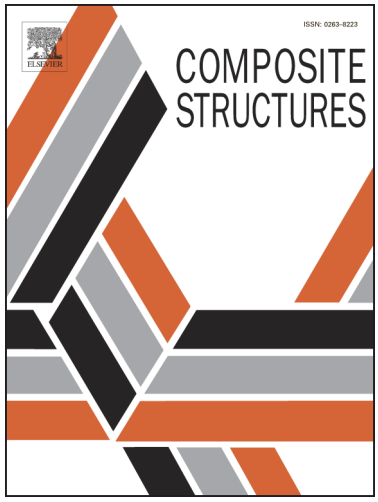

Characterization and physical properties of aluminium foam–polydimethylsiloxane nanocomposite hybrid structures

Susana C. Pinto, Paula A.A.P. Marques, Matej Vesenjak, Romeu Vicente, Luís Godinho, Lovre Krstulović-Opara, Isabel Duarte

PII: S0263-8223(19)33460-9
DOI: https://doi.org/10.1016/j.compstruct.2019.111521
Reference: COST 111521

To appear in: *Composite Structures*

Received Date: 15 September 2019
Revised Date: 30 September 2019
Accepted Date: 2 October 2019

Please cite this article as: Pinto, S.C., Marques, P.A.A., Vesenjak, M., Vicente, R., Godinho, L., Krstulović-Opara, L., Duarte, I., Characterization and physical properties of aluminium foam–polydimethylsiloxane nanocomposite hybrid structures, *Composite Structures* (2019), doi: https://doi.org/10.1016/j.compstruct.2019.111521

Characterization and physical properties of aluminium foam–polydimethylsiloxane nanocomposite hybrid structures

Susana C. Pinto[a], Paula A.A.P. Marques[a], Matej Vesenjak[b], Romeu Vicente[c], Luís Godinho [d], Lovre Krstulović-Opara[e], Isabel Duarte[a].*

[a] Department of Mechanical Engineering, TEMA, University of Aveiro, Aveiro, Portugal

[b] Faculty of Mechanical Engineering, University of Maribor, Maribor, Slovenia

[c] Department of Civil Engineering, RISCO, University of Aveiro, Aveiro, Portugal

[d] Department of Civil Engineering, ISISE, University of Coimbra, Coimbra, Portugal

[e] Faculty of Electrical Eng., Mechanical Eng. and Naval Architecture, University of Split, Croatia

Abstract

This article reports on the fabrication and characterisation of hybrid structures prepared by impregnating an open-cell aluminum foam with polydimethylsiloxane (PDMS) or PDMS reinforced with graphene oxide, GO (PDMS nanocomposite). The effect of the PDMS and the GO on the mechanical, thermal, acoustic absorption and fire retardancy properties of the resulting hybrid structures were evaluated and compared to the individual components (PDMS, PDMS nanocomposite, open-cell aluminium foams). Results demonstrate that the use of the PDMS cured at 65 ºC, as an void filler of the open-cell aluminium foams, changes mechanical and deformation performance, from a rubbery to brittle behaviour, however attaining a higher level of strength (quasi-static: ~5 MPa; dynamic: > 15 MPa) in the resulting hybrid structures. This change is due to the low chain mobility of the polymer and effective adhesion with struts of the open-cell aluminium foams. Furthermore, these hybrid structures are extremely sensitive to strain-rate testing, exhibiting a maximum compressive stress increase of more than 300 % and 200 %, respectively. The presence of the GO within the PDMS improves significantly the non-flammability of the hybrid structures and increases the sound absorption coefficient.

Keywords. Open-cell aluminium foam; Polydimethylsiloxane; Graphene oxide; Hybrid structures; Mechanical and thermal properties; Acoustic absorption

* Corresponding author. Tel.: +351 234 370830;
E-mail: isabel.duarte@ua.pt (Isabel Duarte)

1. Introduction

The search for high-performance lightweight multifunctional materials has increasingly become a target for commercial, industrial and military purposes [**1**]. Solid cellular (porous) materials [**2-3**] and nanocomposites [**4-5**] are examples of these multifunctional materials. Both have tremendous potential to develop high-performance structural components, reducing weight, while improving efficiency, safety and versatility. They offer notable properties and functionalities, which cannot be achieved with common materials that target a specific functional property. The properties of the solid cellular metals result from their porous cellular structures (open or closed cells) together with the properties of the metal they are made of [**6**]. Open-cell foams are used as functional materials, e.g. as filters, batteries, electrodes, heat exchangers and biomedical implants, while the closed-cell foams are used as structural materials as lightweight impact energy and sound absorbers, e.g. in construction, vehicles, devices and other equipment [**7**]. In the last decades, several cellular metals have been developed in order to achieve the control of the size and shape of the cells. It is possible to differentiate two main groups: stochastic and periodic cellular metals [**3**]. Stochastic cellular metals exhibit irregular cellular structures [**8**]. The stochastic cellular metals cannot be characterised by a single unit cell, which makes it difficult to predict their final properties. Closed-cell metal foams prepared by direct [**9**] and indirect [**10**] foaming methods are examples of stochastic foams. To overcome this problem, periodic cellular metals are being developed in order to establish the relationship between the cellular structures and the properties. Syntactic foams are an example of periodic cellular metals with an easily reproducible unit cell, which are prepared by incorporating porous particles or hollow spheres made of ceramic or metal into the metallic matrix [**11-12**]. The porous particles or hollow spheres are packed into a predefined random dense arrangement and a molten metal is infiltrating through the interstitial spaces between the particles or hollow spheres. Periodic cellular structures with complex topologies and graded materials prepared by additive manufacturing technologies (e.g. 3D printing, laser sintering) have been also developed and tested [**13-15**]. Despite their properties can be easily tailored with a specific control of their topologies, some of the tailored cellular metals (density greater than 1g/cm^3) have a higher density

compared to the stochastic foams (density lower than 1g/cm^3) that could limit their application [**16**]. More recently, cellular composites and cellular nanocomposites [**17**] have been developed, in which the metallic bulk matrix is reinforced by micro (e.g. ceramic particles) [**18**] and nano-sized reinforcements (e.g. carbon nanotubes) [**19**] mainly for enhancing the mechanical properties [**17**]. Recently, based on the multi-material concept, hybrid structures have been developed by combining the periodic open-cell aluminium foams [**20-25**] or Advanced Pore Morphology (APM) foam elements [**26-30**] with polymers in which the voids of an open-cell aluminium foams are completely infiltrated with a polymer. Results have demonstrated that the polymer lead to an enhancement of the compressive strength and energy absorption of the resulting hybrid structures compared to the conventional open-cell aluminium foams. The level of enhancement strongly depends on the stiffness of the polymer. The results have revealed that the deformation and failure modes of these hybrid structures strongly depend on the chemical nature of the polymer [**24-25**]. For example, the silicone rubber (gel-like material) promotes non-symmetric deformation, while the brittle epoxy resin promotes symmetric deformation [**24-25**]. Herein, new aluminium foam–polymer hybrid structures were developed, fabricated and analysed to assess their mechanical, thermal, acoustic and fire retardant properties. More specifically, PDMS and PDMS nanocomposites were used as void fillers of open-cell aluminium (Al) foams. The effect of the GO in the polymer matrix on the mechanical, thermal, acoustic and fire retardant properties of the resulting hybrid structures was tested and compared to the individual components (PDMS, PDMS nanocomposite, open-cell aluminium foams).

2. Materials and experimental methods

2.1. Materials

The polydimethilsyloxane (PDMS) Sylgard® 184 was supplied by Dow Corning comprising of two components: a liquid silicone rubber base and a curing agent. An aqueous solution of 4 mg/mL graphene oxide (GO) was provided by Graphenea (Spain). The aqueous suspension was diluted and

lyophilized in order to obtain deagglomerated GO powder. The sheets of GO have a lateral particle size <10 μm and nanometric thickness (monolayer content at about 95%). To prepare the aluminium foam-PDMS (HS) and aluminium foam-PDMS nanocomposite (nHS) hybrid structure specimens, square (22 × 22 × 25 mm^3) and cylindrical (diameter: 37 mm; height: 23 mm) open-cell aluminium foams (OCF) specimens with pore sizes of 10 ppi (pores per inch) were cut from foam blocks made of Al alloy A 356 (AlSi7Mg0.3) (300 × 150 × 150 mm^3), which was supplied by Mayser GmbH & Co. KG (formely M-pore) using the investment casting method [**24**]. Thin walled tubes made of Al alloy AA6060 T66 (0.35–0.60% Mg; 0.3–0.6% Si; 0.1% Cu; 0.1% Mn; 0.05% Cr; 0.15% Zn; 0.1%Ti) with the inner diameter of 22 mm and thickness of 1.5 mm. Cylindrical moulds made of Al alloy AA6060 T66 with the inner diameter of 50 mm and height of 25 mm were also manufactured for acoustic absorption specimens.

2.2. Specimen fabrication

Four different types of square and cylindrical specimens were prepared: dense PDMS specimens, dense PDMS reinforced with 0.25 wt.% GO (nPDMS) specimens, aluminium foam–PDMS hybrid structures (HS) specimens and aluminium foam–PDMS nanocomposite hybrid structures (nHS) specimens. The PMDS specimens were prepared by filling a mould with liquid PDMS mixture prepared by mixing the liquid silicone rubber base with curing agent (component mixing ratio ~ 10:1 in wt.%) in a vacuum chamber for 30 min. After this period, the mould containing the liquid PDMS mixture was placed in a pre-heated furnace and cured at 65 ºC for 4 h. For preparing the nPDMS specimens, the GO was dispersed into the PDMS matrix by ultrasonic and mechanical stirring. For that, the liquid PDMS liquid was first well mixed together with 0.25 wt.% of GO using a mechanical stirrer at 1000 rpm for 1 h. The resulting liquid nPDMS mixture was submitted for 30 min into an ultrasonic bath and then mechanically stirred at 1000 rpm for approximately 1 h. Afterwards, the curing agent was added, mixed and degassed under a vacuum chamber for 30 min. Finally, the resulting liquid nPDMS mixture was

poured into a mould (square or cylindrical), followed by the curing process at 65 ºC for 4 h. Two other loadings of GO were tested, 0.1 and 0.5 wt.%, for comparison. However, it was observed that for 0.5 wt.%, the viscosity of the mixture was high and therefore, many clusters were observed inhibiting the attaining of a good dispersion of GO in the polymer matrix. For 0.1 and 0.25 wt.%, good GO dispersibility was attained in both cases. However, the fire-retardancy properties were obtained only for 0.25 wt.%. The good dispersion of the fillers in the matrix was initially visually observed based on a homogeneous colour of the suspension and later on, by SEM analysis. **Fig. 1** shows the Scanning Electron Microscope (SEM) images of PDMS (**Fig. 1a**) and nPDMS (**Fig. 1b**) matrices assessed by Hitachi TM 4000 Plus using 15 kV voltage with different magnifications. The SEM images clearly show the sheets of the GO (**Fig. 1b**) in the PDMS matrix**.** Earlier works reported the use of a solvent (THF) to disperse the GO nanofiller [31-32] before adding it to the polymer matrix. However, in this case, as we want to keep the process easier, simpler and with low level of incorporation, the incorporation of GO into PDMS matrix was carried out in the powder form.

The hybrid structure (HS and nHS) specimens were prepared by previously inserting an open-cell aluminium foam into the mould, followed by pouring and curing of the liquid polymer mixture (PDMS and nPDMS). The HS or nHS were cured at 65 ºC for 4 h. The resulting HS and nHS were extracted from the mould after the polymer filler cured completely. For easily extracting, the inner surface of the mould was previously cleaned, polished and greased before inserting the open-cell foam specimen. **Fig. 2** shows the fabricated specimens: conventional OCF (**Fig. 2a**), dense PDMS (**Fig. 2b**), dense nPDMS (**Fig. 2c**), HS (**Fig. 2d**) and nHS (**Fig. 2e**).

The average bulk densities for conventional OCF, dense PDMS, dense nPDMS, HS and nHS are: 943 kg/m^3 (std. deviation: 31.1 kg/m^3), 1076 kg/m^3 (std. deviation: 24.8 kg/m^3), 1068 kg/m^3 (std. deviation: 12.1 kg/m^3), 1087 kg/m^3 (std. deviation: 32.3 kg/m^3) and 1090 kg/m^3 (std. deviation: 4.5 kg/m^3), respectively.

2.3. Thermogravimetric analysis

The thermal stability of the PDMS and nPDMS matrices was assessed by a thermogravimetric analyser (Shimadzu TGA-50) at a scanning rate of 10 ºC/min in the temperature range between 30 and 800 ºC under an oxidative atmosphere (air). The mass of the samples was 10 mg.

2.4. Mechanical tests

The compressive behaviour of the HS and nHS specimens and their individual components (PDMS, nPDMS and OCF) were studied using a servo-hydraulic dynamic INSTRON 8801 testing machine (maximum load 50 kN) at crosshead rates of 0.1 mm/s (quasi-static) and 284 mm/s (dynamic). The high-resolution video camera Sony HDR-SR8 and the mid-wave infrared (IR) cooled thermal camera Flir SC 5000 [33] were used in the quasi-static and dynamic tests in order to record the deformation and failure modes of the specimens. The temperature (heat) distribution on the specimen surface and the plastification front propagation can be efficiently observed by IR thermography to detect plastification zones in structures based on cellular metals [33]. The weight, width and height of each specimen were measured to calculate the density (weight/volume). The recorded load-displacement data were converted to stress-strain data. The engineering stress and engineering strain values were determined by dividing the load with the initial cross-section and by dividing the displacement with the initial specimen height, respectively. The energy absorption density (EAD) curves and the specific energy absorption (SEA) values were calculated according to the ISO 13314: 2011 by integrating the engineering stress-strain curves (from 0 up to the maximum strain attained in each test) and by dividing the EAD values by the specimen mass, respectively.

2.5. Thermal tests

The thermal conductivity properties of different types of specimens were evaluated resourcing to a Hot Disk TPS 2500 S instrument using the transient plane source method at room temperature according

to the standard ISO 22007-2.2 [34] and ASTM D7984 [35]. During the experiment, a small constant current is applied to the sensor inserted between two identical specimens. Since the temperature increase of the sensor is highly dependent on the two tested samples attached to it, thermal properties of the tested samples can be determined by monitoring the temperature increase for a short time period. For the measurements one pair of identical samples per material is tested at room temperature and five measurements are conducted for the sake of repeatability.

2.6. Acoustic tests

The sound absorption coefficient and sound absorption efficiency of the OCF, PDMS, nPDMS, HS and nHS specimens was evaluated using an impedance tube according to the standard ASTM E 1050 [36]. The cylindrical specimen was placed into the testing impedance tube with the inner diameter of 37 mm at one end. At the other end of the tube a sound source consisting of a loudspeaker emitting a random noise was introduced. Two microphones were placed into the tube between the sound source and the specimen to detect the sound pressure wave transmitted through the specimen and the portion of the wave that was reflected. The acoustic absorption coefficient (α) is defined as a ratio of absorbed sound intensity in a given material and the incident sound intensity that is imposed on that material. The sound absorption coefficient varies with the frequency. The α varies from 0 (0 % sound absorption) to 1 (100 % sound absorption). The value 0 means no sound is absorbed, while the value 1 means all sound energy is absorbed. For example, a material that has an acoustic absorption coefficient of 0.5 at a given frequency, absorbs half of the sound and either reflects or passes the rest. The materials with a sound absorption coefficient equal to or higher than 0.5 are usually considered efficient sound absorption materials [37]. The noise reduction coefficient (NRC) is another parameter used to evaluate the sound absorption characteristics of a material. The NRC is calculated by defining an average of the sound absorption coefficients at the frequencies 250 Hz, 500 Hz, 1000 Hz and 2000

Hz and rounding off the result to the nearest multiple of 0.05. However, it should be noted that the same value of NRC for two different materials does not mean that they perform in the same way.

2.7. Fire retardancy tests

The fire retardancy tests were based on the direct observation of the specimen behaviour when subjected to a live flame source. The tests consisted of applying an ethanol flame at the specimen's bottom using the set-up in vertical sample position for 3 s plus the subsequent 3 s for observing the self-extinguishing process.

3. Results and discussion

3.1. Thermal properties

Fig. 3 shows the TG (thermogravimetric) and the corresponding DTG (derivative of thermogravimetric) curves of PDMS and nPDMS samples in air. The shape of the TG/DTG curves is identical for both PDMS and nPDMS specimens. From room temperature to 270 °C, the weight loss is negligible. Then two distinct degradation steps were observed. After an initial gradual weight loss, a significant weight loss was observed above 400 °C, corresponding to a high peak in the DTG curves. After ~600 °C, the weight loss remained constant. The total weight loss of PDMS and nPDMS was 49.5% and 48.3%, respectively. Both specimens showed a two-stage degradation processes in which DTG curves show the initial peak at 349 ºC and 336 ºC, followed by the next peak at 519 ºC and 528 ºC for the PDMS and nPDMS, respectively. This two-stage oxidative degradation process was reported by Camino et al. [**38**]. They proposed that the oxygen catalyses the depolymerization reaction of PDMS to volatile cyclic oligomers, leading to a lower temperature when the weight starts to decrease. The small difference in the TG/DTG curves is due to the interaction between the GO and the molecule chains of silicon rubber. It seems to decrease the total weight loss of the resulting PDMS

nanocomposites. With the addition of the GO, the maximum DTG is attained at a higher temperature (528 ºC), suggesting a slight improvement in the thermal stability.

3.2. Compressive behaviour

3.2.1. Compression behaviour of PDMS and PDMS nanocomposite specimens

Fig. 4 shows the compressive deformation and failure modes (**Fig. 4a**) and the stress-strain curves (**Fig. 4b**) of dense PDMS and nPDMS specimens subjected to quasi-static and dynamic loading conditions.

The results clearly show that the deformation and failure modes of the PDMS changed due to the presence of the GO within the polymer matrix (**Fig. 4a**) and due to the loading velocity. Under quasi-static compression, the PDMS exhibited a symmetric deformation, showing a barrelling effect of the inner surface of the specimen, accompanied by the appearance and propagation of several internal cracks during the uniaxial compression, followed by the brittle failure of the specimens (quasi-static loading, **Fig. 4a**). On the other hand, the nPDMS under quasi-static compression displayed an initial symmetric deformation that changed to an unstable non-symmetric deformation accompanied by the tilting of the upper surface of the specimen during loading (strains above 0.5, **Fig. 4a**), followed by the brittle failure of the specimens leading to its disintegration. From IR image sequences for the PDMS and nPDMS under dynamic loading conditions (**Fig. 4a**), it can be concluded that the specimens deform and fail in a identical mode. However, very different behaviour was observed in comparison to quasi-static loading condition of the same specimen types (**Fig. 4a**). No tilting of the specimens was observed during the compression tests performed under dynamic loadings as it was the case for the nPDMS specimen compressed under quasi-static loading conditions. The deformation and failure modes of the PDMS and nPDMS specimens are directly related to the diagram shape of the measured stress–strain curves (**Fig. 4)**.

The shape of the PDMS and nPDMS curves is similar (**Fig. 4b**) and can be divided into three main regions: initial linear elastic response in the regime of small strain values, followed by a nonlinear

increase in terms of stress up to the maximum compressive stress (peak stress) and a sudden drop of stress before final failure. The region, after post-peak values were attained, this is when the stress starts to drastically decrease, is characterized by unstable oscillations in stress, namely for the cases of specimens that were subjected to dynamic loading conditions.

The experimental results also reveal that PDMS and nPDMS are highly sensitive to strain imposed rate, exhibiting an obvious positive strain rate sensitivity. The dynamic compressive curves (red curves, **Fig. 4b**) of PDMS and nPDMS are much higher in comparison to the curves at quasi-static loading (black curves, Fig. 4b). For example, the peak stresses for PMDS specimens are 32.91 MPa (quasi-static) and 71.42 MPa (dynamic), while for nPDMS specimens, they are 30.21 MPa (quasi-static) and 54.92 MPa (dynamic), as shown in **Table 1**. These represent percentage increases of 117 % and 82 % for PMDS and nPDMS specimens, respectively.

From these experimental results, it could be also noticed that the PMDS specimens present a higher compressive strength compared to the nPDMS. After the first peak stress (**Fig. 4b**), the PDMS and nPDMS specimens subjected to the quasi-static loading conditions quickly dropped to very low values of stress (PDMS: ~1.16 MPa; nPDMS: ~1.22 MPa) without stress oscillations, while the specimens subjected to the dynamic loading conditions exhibited several stress oscillations. Clearly, the compressive behaviour of the PDMS specimens subjected to the dynamic loading was changed with the presence of the GO within the PDMS matrix. The presence of the GO leads to lower values of the peak stress but provides for a recoverable deformation after the first peak value of stress, showing a strong non-linear behaviour. For the nPDMS specimens, the stress increases (~12.95 MPa) up to the strain of ~0.7 (**Fig. 4b**). The mechanical response of these specimens is related to their chemical nature [**38-41**]. As it well known, the mechanical response of a polymer depends on the temperature, strain rate and loading conditions. In particular, the mechanical response of most polymer rubbers (e.g. PDMS) may change from rubbery (elasticity) to ductile (plasticity) or even to brittle due to temperature and strain rate changes**.** These polymers usually exhibit large and recoverable strain hardened

deformation. In fact, the PDMS became softer and could be compressed further without fracture and failure. Such unique mechanical properties of elastomers are related to the 3D network structure (comprising of long and flexible polymer chains) that is characterized by several parameters, such as the length of the network strands, functionality of cross-links and the number of entanglements, dangling chains and loops. The PDMS is considered as one of the most flexible polymers. Their high flexibility can be explained by the structural features of the Si–O bonds that have a longer bond length, larger bond angle and significantly lower torsional potential than C–C bonds. This leads to a very low glass transition temperature for the PDMS. The PDMS experiences crystallization at substantially low temperatures (below 30 ºC). No strain-induced crystallization at room temperature is observed for the cross-linked PDMS and they behave as elastomers. The mechanical strength of the specimens was enhanced by decreasing the hybrid structure density. The drop-in stress for dense specimens subjected to dynamic loading conditions is much lower (PDMS: 42 %; nPDMS: 36.9 %) compared to those subjected to quasi-static loading conditions (PDMS: 96.5 %; nPDMS: 96 %).

3.2.2. Compression behaviour of open-cell aluminium foams

The compressive deformation and failure modes (**Fig.5a**) and stress-strain curves (**Fig. 5b**) of OCF specimens are shown in **Fig. 5**.

As expected, the compressive response of OCF specimens is divided into three regions [**24**]: elastic, plateau and densification. In the initial elastic region, the deformation of the foam is controlled by the deformation of the pore walls due to bending and buckling, followed the plateau region, where the foam exhibits a long (almost) constant stress due to progressive layer-by-layer collapse (plastic deformation, buckling, fracture and brittle collapse). Finally, the foam densifies due to the contact between the cell struts, exhibiting an abrupt increase of the stress. In fact, the OCF starts to deform at weak points (IR images, **Fig. 5a**), followed by a band formation. The stress fluctuations are observed in the plateau region (**Fig. 5b**) due to their layer-wise brittle collapse [**17**]. These results (**Fig. 5b**)

confirm our previous findings [**24**] that the Al alloy OCF is slightly sensitive to the strain rate, in which the dynamic curves (red curves) are slightly superior (higher peak stresses) in comparison to the quasi-static ones (black curves).

3.2.3. Compression behaviour of aluminium foam – PDMS and aluminium foam – PDMS nanocomposite hybrid structures

Fig. 6 shows the compressive deformation and failure modes (**Fig.6a**) and stress-strain curves (**Fig. 6b**) of the HS and nHS specimens.

The dynamic failure and deformation modes of the HS and nHS specimens were also studied using the IR thermography. The experimental results confirm that the presence of the polymer filler (PDMS and nPDMS) in the voids of the OCF changes the deformation behaviour and failure modes of the OCF characterized by layer-wise collapse. The polymer filler prevents the self-contact of struts. Additionally, no deformation bands are visible. The PDMS and nPDMS promotes symmetric deformation in HS and nHS specimens by folding in the middle at both (quasi-static and dynamic) loading conditions as can be seen in **Fig. 6a**. The HS and nHS hybrid structures exhibit a brittle behaviour under compressive loads, leading to the development of cracks during the so-called, fold formation (i.e. barrelling in the central section of the specimens). Furthermore, the deformation and failure modes of the HS and nHS specimens are completely different from those observed in identical hybrid structures developed and studied in previous work carried out [**24**]. In [**24**], hybrid structures specimens were prepared by impregnating the same OCF as used in this study, with PDMS cured at room temperature for 24 h (designated by HS-R). Herein, the HS and nHS specimens were prepared by infiltrating the OCF with PDMS and cured at 65 ºC for 4 h. Obviously, the difference of the deformation and failure modes between the HS and HS-R specimens is due to the thermal curing cycle during fabrication. The PDMS changes from rubbery [**24**] to brittle (**Fig. 6a**) when subjected to different curing temperatures, i.e. from room temperature to 65 ºC, respectively. Therefore, the HS and

HS-R specimens exhibit a rubber-like and brittle behaviour, respectively. This is related to the chemical nature of the PDMS, where the silicon atoms are linked to carbon, hydrogen and oxygen atoms. Their structural features, such as Si–O–Si angles, Si–O bond length, dissociation energy, the freedom of rotation and the weak intermolecular forces among polymer chains with a high chain mobility make them very flexible with unique physical (mechanical and thermal) and chemical properties. A low adhesion between the silicone and the struts of the OCF and a lower friction coefficient is observed in the HS-R specimens as reported by Duarte et al. [**24-25**]. Furthermore, the silicone rubbers behave in comparison differently to the other polymers, since their structure is highly deformable and self-restoring. Published results have demonstrated that the mechanical properties of silicone increases with the increasing of the curing time. Therefore, the brittleness of HS and nHS specimens might be a result of the high curing temperature (65 ºC) used in their fabrication, leading to a high adhesion between the silicone and the struts of the OCF, diminishing its chain mobility. The deformation and failure modes of the HS and nHS specimens are identical to the OCF specimens embedded with brittle epoxy resin [**24**], displaying a negligible chain mobility. The epoxy resin promotes a symmetric deformation in the resulting hybrid structures at both (quasi-static and dynamic) loading conditions, as in the case of the HS and nHS specimens. On the other hand, the HS-R experienced a non-symmetric deformation [**24**] for both (quasi-static and dynamic) loading conditions. In this case, the Si–O bonds are longer with fewer alkyl groups than C–C bonds, these shows a lower mechanical strength compared to the HS prepared in this study. **Fig. 6b** shows the compressive stress-strain curves of the HS and nHS specimens for both (quasi-static and dynamic) loading conditions. The HS and nHS hybrid structures are significantly more sensitive to strain rate than the HS-R and the OCF [**24**]. The dynamic curves of HS and nHS specimens (red curves) are much higher in comparison to the quasi-static curves (black curves), as shown in **Fig. 6b.** For example, the values of the first peak stress attained, change from 5.25 MPa (quasi-static, **Table 2**) to 13.94 MPa (dynamic, **Table 2**) and from 4.93 MPa (quasi-static, **Table 2**) to 12.97 MPa (dynamic, **Table 2**) for HS and nHS specimens,

respectively. Results in this field have demonstrated that some others cellular metals have showed only a slight strain-rate sensitivity, where the dynamic response was only slightly above the quasi-static response for moderate dynamic loading velocities (284 mm/s) [**24, 25, 42**]. For example, the values of the first peak stress of the OCF change from 0.28 MPa to 0.31 MPa for the quasi-static and dynamic loading conditions. However, the dynamic response of the HS-R is below the quasi-static response [**24**], in the initial region up to strain of ~0.2. The HS and nHS specimens exhibit a significantly higher level of compressive stress, reaching a stress value of 5 MPa and over 20 MPa for quasi-static and dynamic loading conditions, respectively (**Fig. 6b**).

The diagram shape of the compressive stress-strain curves of the HS and nHS specimens differ from the curves of HS-R specimens. This is attributed to the different characteristics of the polymers that are subjected to different curing temperature, as described above. Results also indicated that the diagram shape depends on the (quasi-static and dynamic) loading conditions. The diagram shape of quasi-static curves for the HS and nHS specimens is divided into the following four regions: the initial linear elastic, followed by a nonlinear increase in stress up to the maximum compressive stress, drop in stress and a visible recoverable deformation. However, the diagram shape of dynamic curves for the HS and nHS specimens can be divided into the following regions: the initial linear elastic region, followed by a nonlinear increase in stress up to the first peak stress, followed by a minor drop in stress to a given minimum stress value, followed by a stress fluctuation exhibiting a sequence of peaks reaching the maximum compressive stress before the failure. For example, the HS specimens reached the first peak stress of 13.92 MPa (at strain of 0.45), followed the recoverable deformation, reaching the maximum compressive stress of 42 MPa (at strain of 0.8). These experimental results show that the HS and nHS exhibit large and recoverable strain hardening deformation. The HS and nHS do not display the typical plateau-stress response, exhibiting by the HS-R and conventional OCF specimens (**Fig. 5b**). Moreover, the silicone in the HS-R effectively smoothens and stabilizes the response of the OCF specimens, decreasing the stress oscillations in the plateau region and increasing the values of

their mechanical properties. The compressive stress-strain responses of the HS and nHS specimens (**Fig. 4a**) are inferior to the dense PDMs and nPDMS specimens (**Fig. 6a**). The measured hardness of the PDMS samples also increased linearly with increasing the curing temperature. The compressive responses of the hybrid structures increase by decrease of the OCF's density. The presence of the GO within the PDMS matrix effectively smoothens and stabilizes the response of the HS, decreasing the stress oscillations, achieving similar values of the first peak stress and the maximum compressive stress.

3.2.4. Energy absorption capabilities

The EAD for the HS and nHS specimens in comparison to the individual components (OCF, nPDMS and PDMS) is shown in **Fig. 7**. The dynamic EAD curves of HS and nHS specimens are higher in comparison to the PDMS and nPDMS specimens.

From **Fig. 7**, it can be observed that the HS and nHS specimens are the ones that present higher capacity of EAD. The quasi-static and dynamic EAD curves of the HS and nHS specimens are above the curves of the individual components (PDMS, nPDMS and OCF). At a strain value of 0.5, the HS and nHS are approximately 4 times and 6 times higher in comparison to the OCF specimens subjected to the quasi-static and dynamic loading conditions, respectively. Furthermore, above strain of 0.4, the SEA curves of HS and nHS specimens are also above the ones of individual components (PDMS, nPDMS and OCF), indicating that the HS and nHS have a higher energy absorption capacity.

3.3. Thermal insulation

The effects of the presence of the polymer in the voids of the OCF and the presence of the GO within the polymer matrix on the thermal conductivity is shown in **Fig. 8**. As expected, the OCF specimens present higher thermal conductivity (1.611 W/(mK)), while the dense the PDMS and nPDMS show lower values (0.181 W/(mK) and 0.187 W/(mK)). The thermal conductivity of the PDMS specimens

(0.181 W/(mK)) are in accordance with values reported in literature (0.15-0.20 W/(mK)) [**43**]. Results indicate that the presence of the GO within the polymer matrix has a positive effect on the thermal conductivity. For example, the thermal conductivity increases from 0.181 W/(mK) to 0.187 W/(mK) for dense PDMS and nPDMS specimens, leading to an increase of approximately 3.5 %. The main reasons for this include: (i) the percentage of incorporation of the GO (0.25wt.%) within the PDMS matrix is very low for allowing the formation of a conducive network that will provide an effective pathway for the phonon movement in the insulator matrix, leading to higher thermal conductive values, (ii) even for low levels of incorporation, the formation of aggregates may occur, which restricts the heat transport. In fact, aggregates reduce the aspect ratio, decrease the contact area and trap or scatter phonons. Similar studies that describe the incorporation of carbon nanostructures drive special attention towards the uniform dispersion of fillers in the matrix in order to reduce the mismatch by reducing the interfacial resistance. Similar positive effect is also observed in the hybrid structures in which the effective thermal conductivity increases from 0.241 (HS) to 0.291 W/(mK) (nHS). From these experimental results, it can be observed that the thermal conductivities of the OCF (1.611 W/(mK)) significantly decreased when the voids are filled by polymers (PDMS and nPDMS). The presence of an Al network structure facilitates the heat transfer.

3.3. Acoustic absorption

The sound absorption coefficient curves of hybrid structures (HS and nHS) and the individual components (PDMS and nPDMS) are presented in **Fig. 9**. Herein, the effect of the PDMS and the GO on the acoustic absorption properties is shown.

As described above, the PDMS is a semi-crystalline thermoplastic polymer composed of a chain of alternating silicon and oxygen atoms. Each silicone has two methyl groups attached to it by Van der Waal's forces. The main intermolecular interactions between the chains are weak forces. Their structure is long with highly flexible chains, resulting in rubber-like elasticity. Moreover, the PDMS

exhibits both elastic and viscous properties. This means that it acts like a viscous liquid (e.g. honey) or an elastic solid (e.g. rubber) when subjected to high and low temperatures, respectively. Moreover, when the PDMS chains undergo vibrations, part of the energy is stored (elastic) and part is dissipated as heat (viscous) within the polymer. This viscous nature results in loss of vibration energy as heat, consequently enhancing the sound absorption [44]. The incorporation of the GO within the PDMS matrix, create voids in the PDMS matrix, as observed by SEM (**Fig. 1**) and as suggested in the compression tests, leading to an increase in the sound absorption. In this case, an increase of approximately 80 % in the frequency range from 500 Hz to 1250 Hz was observed. The enhancement of sound absorption coefficient of foamed materials impregnated with carbon nanoparticles was also reported by other authors [45]. This could be attributed to the large surface of the GO sheets that can be responsible for the dissipation by interfacial sliding and stick-slip behaviour. In the case of the HS, an enhancement in the sound absorption was also observed, due to the voids created around the metal skeleton. A peak increase of more than 150 % was observed for the HS in comparison to the PDMS. The better sound absorption was obtained for nHS with values around 0.5 at frequency of 1000 Hz.

The comparison with other reported results in literature is not simple, since there are limited studies reporting on sound absorption of this type of composites [**44-45**]. It is well known that sound waves propagate fast in solid materials, contrary to fluids. When the sound wave hits a solid surface, the material vibrates, the molecules that compose the material collide one another and the kinetic energy is passed from molecule to molecule. Furthermore, the transmission of energy is higher when molecules are closer to each other and stronger bonded [**46**]. As so, the dense materials are not widely used for sound absorbers like foamed materials. However, they are used as coatings or sheets to dampen vibrations and sound [**47**].

3.4. Fire retardancy properties

The effect of the GO on the fire retardancy properties of the nPDMS was evaluated. **Fig. 10** shows the sequence image for the PDMS and nPDMS specimens. As expected, the PDMS matrix exhibited a rapid and complete combustion, along with extensive dripping from the specimens. The incorporation of the GO within the PDMS matrix results in a significant reduction of the PDMS flammability, as shown in **Fig. 10**. No flame is observed for the nPDMS, while the flame for the PDMS extinguishes after 5 s. Similar results were observed previously for polymer nanocomposites [48]. It has been demonstrated that carbon nanostructures are efficient for the elastomers in terms of fire retardancy. In specific conditions, the accumulation of nanoparticles in polymer is beneficial to avoid the flow of the molten polymer and consequent physical defects in the protecting layer.

4. Conclusions

Aluminium foam– polydimethylsiloxane (PDMS) and aluminium foam–PDMS nanocomposite hybrid structures (HS and nHS) were developed by impregnating an open-cell aluminium foam (OCF) with PDMS or PDMS reinforced with graphene oxide (PDMS + GO = nPDMS), respectively. The thermal curing cycle lasted at 65 ºC for 4 h. The mechanical, thermal, acoustic absorption and fire retardancy properties of the hybrid structures were compared to the individual components (PDMS, nPDMS and OCF). Results demonstrate that the compressive response, e.g. the shape of the stress-strain curves, deformation behaviour and failure modes, of hybrid structures is notably influenced by the curing temperature of the PDMS. The mechanical response of the PDMS may change from rubbery to brittle via ductile plasticity by the thermal curing cycle, in particular the curing temperature. The use of high curing temperature (65 ºC) of the silicone leads to a brittle behaviour of the resulting hybrid structure reaching a high level of strength (quasi-static: ~5 MPa; dynamic: > 15 MPa), due to the low chain mobility of the polymer and high adhesion between the struts of the OCF. Contrary, the use of the low temperature (room temperature) leads to a rubbery behaviour of the hybrid structure reaching a low

level of compressive strength (~0.47 MPa), due to the high chain mobility of the polymer and low adhesion between the silicone and the struts of the OCF.

The HS and nHS specimens with brittle behaviour are extremely sensitive to the strain rate imposed compared to other cellular metals and hybrid structures based on silicone cured at room temperature. The HS and nHS specimens exhibited a compressive stress increase of more than 300 % and 200 %, respectively. The silicone with rubbery behaviour (gel-like material) promotes non-symmetric deformation in the hybrid structure specimens, while the silicone with brittle behaviour promotes symmetric deformation in the HS and nHS specimens by barrelling in the middle of the specimens for both (quasi-static and dynamic) loading conditions. The hybrid structure prepared by high curing temperature (65 ºC) exhibited a brittle behaviour under compressive loads, leading to the development of cracks during the fold formation (i.e. barrelling in the centre of the specimens).

Results also demonstrate that the presence of the GO within the PDMS matrix (even as low as 0.25 wt.%) provides voids in the nHS, which efficiently increase the sound absorption coefficient of 0.5 at frequency of 1000 Hz. Furthermore, the incorporation of the GO into PDMS matrix shifted the maximum DTG to higher temperature, suggesting a slight improvement in the thermal stability. The presence of the GO within the PDMS matrix also ensured that the hybrid structure was able to significantly mitigate and assure a fairly good non-flammable behaviour.

Acknowledgments

This work was supported by the Portuguese Foundation for Science and Technology (FCT) under the Grant SFRH/BD/111515/2015 and to the projects UID/EMS/00481/2019-FCT and CENTRO-01-0145-FEDER-022083 - Centro Portugal Regional Operational Programme (Centro2020), under the PORTUGAL 2020 Partnership Agreement, through the European Regional Development Fund. The financial support from the research programme P2-063 entitled “Design of Cellular Structures” funded by the Slovenian Research Agency “ARRS” is gratefully acknowledged.

References

[1] A.D.B.L. Ferreira, P.R.O. Nóvoa, A.T. Marques. Multifunctional Material Systems: A state-of-the-art review. Composite Structures 2016. 151. 3-35.

[2] J. Banhart. Manufacture. characterisation and application of cellular metals and metal foams. Progress in Materials Science 2001. 46 (6). 2001. 559-632.

[3] I. Duarte, N. Peixinho, A. Andrade-Campos, R. Valente. Editorial – Special Issue on Cellular Materials. Science and Technology of Materials 2018; 30: 1–3.

[4] S.C. Tjong. Structural and mechanical properties of polymer nanocomposites. Materials Science and Engineering: R: Reports 2006. Volume 53. Issues 3–4. 30 August 2006. Pages 73-197.

[5] S.C Tjong. Recent progress in the development and properties of novel metal matrix nanocomposites reinforced with carbon nanotubes and graphene nanoplates. Materials Science and Engineering: R: Reports 2013. 74: 281-350.

[6] H.-P. Degischer; B. Kriszt. Handbook of Cellular Metals: Production. Processing. Applications. Copyright © 2002 Wiley-VCH Verlag GmbH & Co. KGaA.

[7] F. Garcia-Moreno. Commercial Applications of Metal Foams: Their Properties and Production. Materials (Basel). 2016 Jan 29;9(2). pii: E85. doi: 10.3390/ma9020085.

[8] M. Ulbin, M. Vesenjak, M. Borovinšek, I. Duarte, Y. Higa, K. Shimojima, Z. Ren. Detailed Analysis of Closed-Cell Aluminum Alloy Foam Internal Structure Changes during Compressive Deformation. Adv. Eng. Mater. 2018. 20 (8). Article number 1800164. doi:10.1002/adem.201800164.

[9] T. Miyoshi. M. Itoh. S. Akiyama. A. Kitahara. ALPORAS Aluminum Foam: Production Process. Properties. and Applications. Advanced Engineering Materials 2000. 2(4): 179-183.

[10] I. Duarte, JMF Ferreira. 2D quantitative analysis of metal foaming kinetics by hot-stage microscopy. Advanced Engineering Materials 2014, 16: 33-39.

[11] I.N. Orbulov. A. Szlancsik. On the Mechanical Properties of Aluminum Matrix Syntactic Foams. Advanced Engineering Materials. 20(5).1700980

[12] Taherishargh. M. Katona. B. Fiedler. T. Orbulov. I.N. Fatigue properties of expanded perlite/aluminum syntactic foams. Journal of Composite Materials 2017. 51(6): 773-781.

[13] Wadley. H.N.G. Multifunctional periodic cellular metals. Phil. Trans. R. Soc. A (2006) 364. 31–68.

[14] N. Novak, M. Vesenjak, Z. Ren. Auxetic Cellular Materials – a Review. Journal of Mechanical Engineering 2016, 62(9): 485-493.

[15] N. Novak, L. Starčevič, M. Vesenjak, Z. Ren. Blast response study of the sandwich composite panels with 3D chiral auxetic core. Composite Structures 2019, 210: 167-178.

[16] N. Gupta. P.K. Rohatgi (Eds.). Metal Matrix Syntactic Foams: Processing. Microstructure. Properties and Applications. DEStech Publications Inc.

[17] I. Duarte, JMF Ferreira. Composite and nanocomposite metal foams. Materials 2016. 9(2).79.

[18] Liu. J.; Yu. S.; Zhu. X.; Wei. M.; Li. S.; Luo. Y.; Liu. Y. Correlation between ceramic additions and compressive properties of Zn-22 Al matrix composite foams. Journal of Alloys and Compounds 2009, 476: 220–225.

[19] I. Duarte, E. Ventura, S. Olhero, JMF Ferreira. A new class of closed-cell aluminium foams reinforced with carbon nanotubes. Ciencia e Tecnologia dos Materiais. 28(1): 5-8.

[20] M. Vesenjak. L. Krstulović-Opara. Z. Ren. A. Öchsner. Ž. Domazet. Experimental Study of Open-Cell Cellular Structures with Elastic Filler Material. Exp. Mech. 49 (2009) 501–509.

[21] M. Vesenjak. L. Krstulović-Opara. Z. Ren. Z. Domazet. Cell shape effect evaluation of polyamide cellular structures. Polymer Testing 2010, 29: 991–994.

[22] M. Vesenjak. L. Krstulović-Opara. Z. Ren. Characterization of photopolymer cellular structure with silicone pore filler. Polym. Testing 31 (2012) 705–709.

[23] M. Vesenjak. L. Krstulović-Opara. Z. Ren. Characterization of irregular open-cell cellular structure with silicone pore filler. Polym. Test. 32 (2013) 1538–1544.

[24] I. Duarte. M. Vesenjak. L. Krstulović-Opara. Z. Ren. Crush performance of multifunctional hybrid foams based on an aluminium alloy open-cell foam skeleton. Polymer Testing 2018; 67: 246–256.

[25] I. Duarte. M. Vesenjak. L. Krstulović-Opara. J. Dias-de-Oliveira. M. Vesenjak Axial crush performance of polymer-aluminium alloy hybrid foam filled tubes. Thin-walled Structures 2019. 138. 124-136.

[26] M. Reinfried. G. Stephani. F. Luthardt. J. Adler. M. John. A. Krombholz. Hybrid foams – a new approach for multifunctional. Applications. Adv. Eng. Mater. 13 (2011) 1031-1036.

[27] K. Stöbener. G. Rausch. Aluminium foam–polymer composites: processing and characteristics. J. Mater. Sci. 44 (2009) 1506–1511.

[28] L. Carrino. M. Durante. S. Franchitti. L. Sorrentino. Mechanical performance analysis of hybrid metal-foam/composite samples. Int. J. Adv. Manuf. Technol. 60 (2012) 181–190.

[29] S. Kishimoto. Q. Wang. Y. Tanaka. Y. Kagawa. Compressive mechanical properties of closed-cell aluminium foam–polymer composites. Composites Part B 64 (2014) 43–49.

[30] J. Yuan. X. Chen. W. Zhou. Y. Li. Study on quasi-static compressive properties of aluminium foam-epoxy resin composite structures. Composites Part B 79 (2015) 301–310.

[31] M. Panahi-Sarmad, E. Chehrazi, M. Noroozi, M. Raef, M. Razzaghi-Kashani, and M. A. Haghighat Baian. Tuning the Surface Chemistry of Graphene Oxide for Enhanced Dielectric and Actuated Performance of Silicone Rubber Composites. ACS Appl. Electron. Mater. 1 (2019) 198–209.

[32] R. Niu, J. Gong, D. Xu, T. Tang, and Z.-Y. Sun. Influence of molecular weight of polymer matrix on the structure and rheological properties of graphene oxide/polydimethylsiloxane composites. Polymer 55 (2014) 5445–5453.

[33] L. Krstulović-Opara, M. Vesenjak, I. Duarte, Z. Ren, Z. Domazet. Infrared Thermography as a Method for Energy Absorption Evaluation of Metal Foams. Materials Today Proceedings. 3 (2016) 1025–1030.

[34] ISO 22007-2.2. Plastics - Determination of thermal conductivity and thermal diffusivity - Part 2: Transient plane heat source (hot disc) method.

[35] ASTM D7984 Standard Test Method for Measurement of Thermal Effusivity of Fabrics Using a Modified Transient Plane Source (MTPS) Instrument thermal.

[36] ASTM E1050-12 Standard Test Method for Impedance and Absorption of Acoustical Materials Using a Tube, Two Microphones and a Digital Frequency Analysis System.

[37] The materials with a sound absorption coefficient equal to or greater than 0.5 are usually considered efficient sound absorption materials

[38] G. Caminoa, S.M. Lomakinb, M. Lazzari. Polydimethylsiloxane thermal degradation Part 1. Kinetic aspects, Polymer 2001, 42: 2395-2402

[39] C. R. Siviour, J. L. Jordan. High Strain Rate Mechanics of Polymers: A Review. Journal Dynamic Behavior Material 2016, 2:15–32.

[40] K. Urayama, T. Kawamura, S. Kohjiy, Structure–mechanical property correlations of model siloxane elastomers with controlled network topology. Polymer 2009, 50: 347–356.

[41] W.S. Lee, K.S. Yeo, A. Andriyana, Y.G. Shee, F.R. Mahamd Adikan. Effect of cyclic compression and curing agent concentration on the stabilization of mechanical properties of PDMS elastomer. Materials and Design 96 (2016) 470–475.

[42] I. Duarte, L. Krstulović-Opara, M. Vesenjak, Axial crush behaviour of the aluminium alloy in-situ foam filled tubes with very low wall thickness. Composite Structures 2018, 192: 184-192.

[43] J.E. Mark. Polymer Data Handbook. 2nd edition. Oxford University Press, 2009.

[44] A. Mata, A. J. Fleischman, and S. Roy. Characterization of Polydimethylsiloxane (PDMS) Properties for Biomedical Micro/Nanosystems. Biomedical Microdevices 2005, 7 (4): 281–293.

[45] J. M. Kim, D. H. Kim, J. Kim, J. W. Lee, and W. N. Kim. Effect of graphene on the sound damping properties of flexible polyurethane foams. Macromolecular Research 2017, 25 (2): 190–196.

[46] V. G. Geethamma, R. Asaletha, N. Kalarikkal, and S. Thomas. Vibration and sound damping in polymers. Resonance 2014, 19 (9): 821–833.

[47] N. N. Najib, Z. M. Ariff, A. A. Bakar, and C. S. Sipaut, Correlation between the acoustic and dynamic mechanical properties of natural rubber foam: Effect of foaming temperature, Materials Design 2011, 32 (2): 505–511.

[48] P. S. Khobragade, D.P. Hansora, Jitendra B. Naik, Aniruddha Chatterjee. Flame retarding performance of elastomeric nanocomposites: A review. Polymer Degradation and Stability 2016, 130: 194–244.

Figure Captions

Fig. 1. SEM images of the matrices of PDMS (a) and nPDMS matrices (b).

Fig. 2. Square and cylindrical specimens: OCF (a), dense PDMS (b), nPDMS (c), HS (d) and nHS (e).

Fig. 3. TG/DTG of the PDMS and nPDMS matrices.

Fig. 4. Compressive deformation (a) and stress-strain curves (b) of dense PDMS and nPDMS specimens at quasi-static and dynamic loading conditions.

Fig. 5. Compressive deformation (a) and stress-strain curves (b) of OCF specimens.

Fig. 6. Compressive deformation (a) and stress-strain curves (b) of the HS and nHS specimens.

Fig. 7. Averaged EAD and SEA curves for quasi-static and dynamic loading conditions.

Fig. 8. Thermal conductivity of the hybrid structures (HS and nHS) and the individual components (PDMS, nPDMS and OCF). The error bars show the standard deviation between five replicate tests.

Fig. 9. Sound absorption coefficient curves of the hybrid structures (HS and nHS) and the individual components (PDMS, nPDMS and OCF).

Fig. 10. Fire retardancy sequence image for the PDMS and nPDMS.

Table Captions

Table 1. Compressive results of PDMS and nPDMS specimens.

Table 2. Compressive results of HS and nHS specimens.

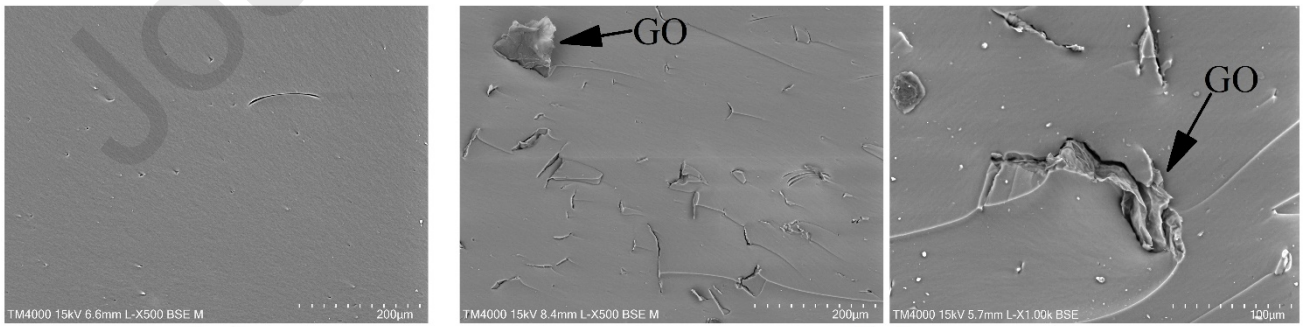

(a) (b)

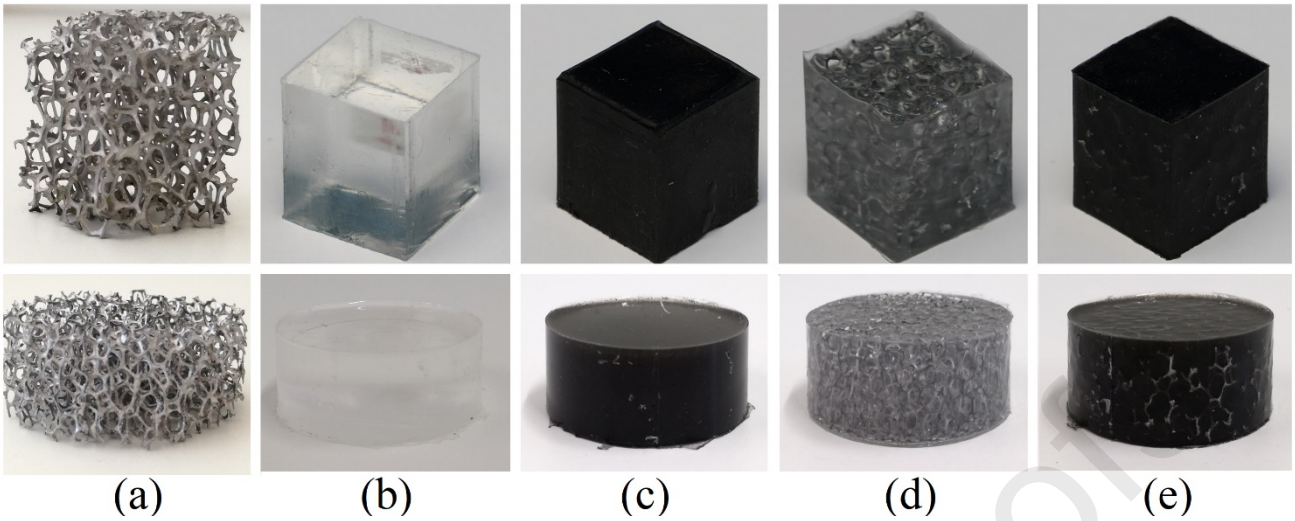

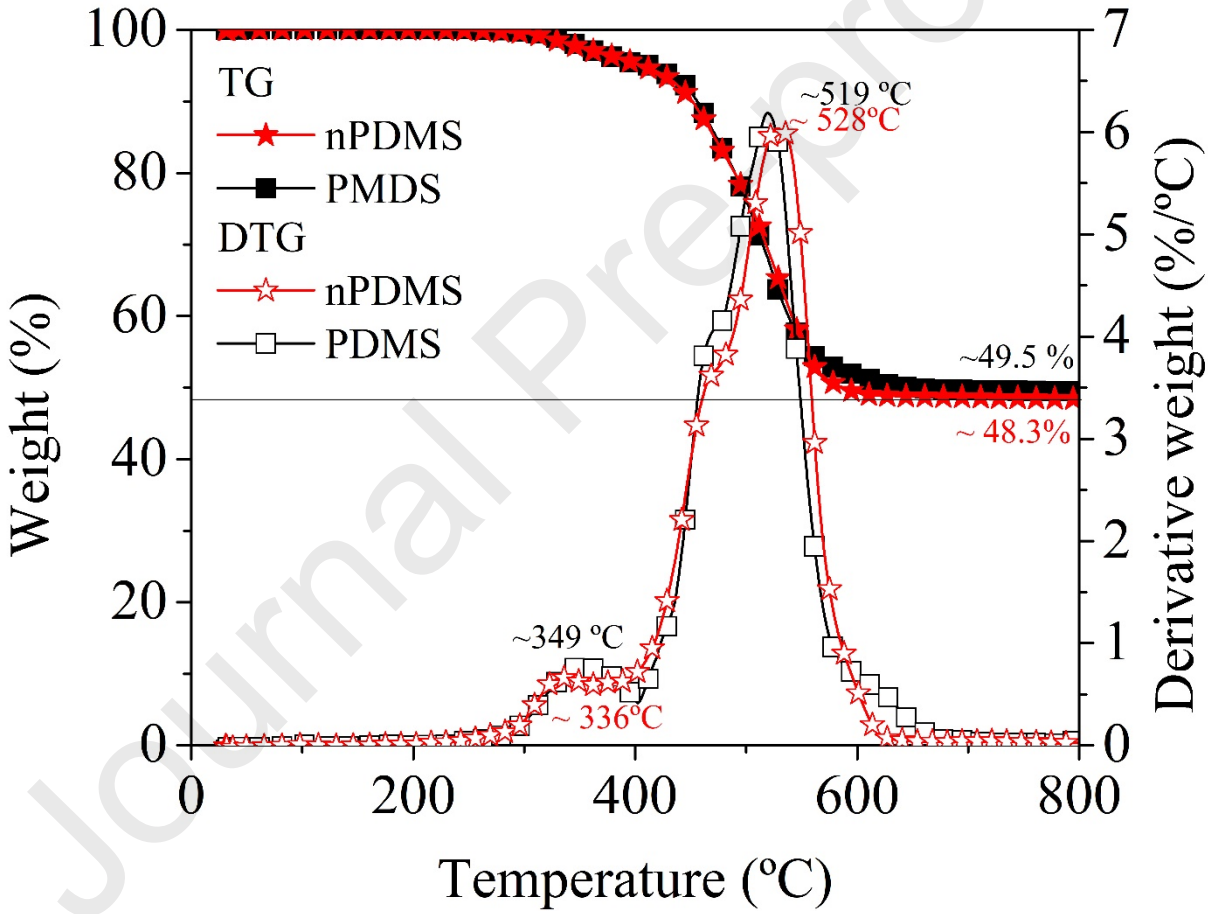

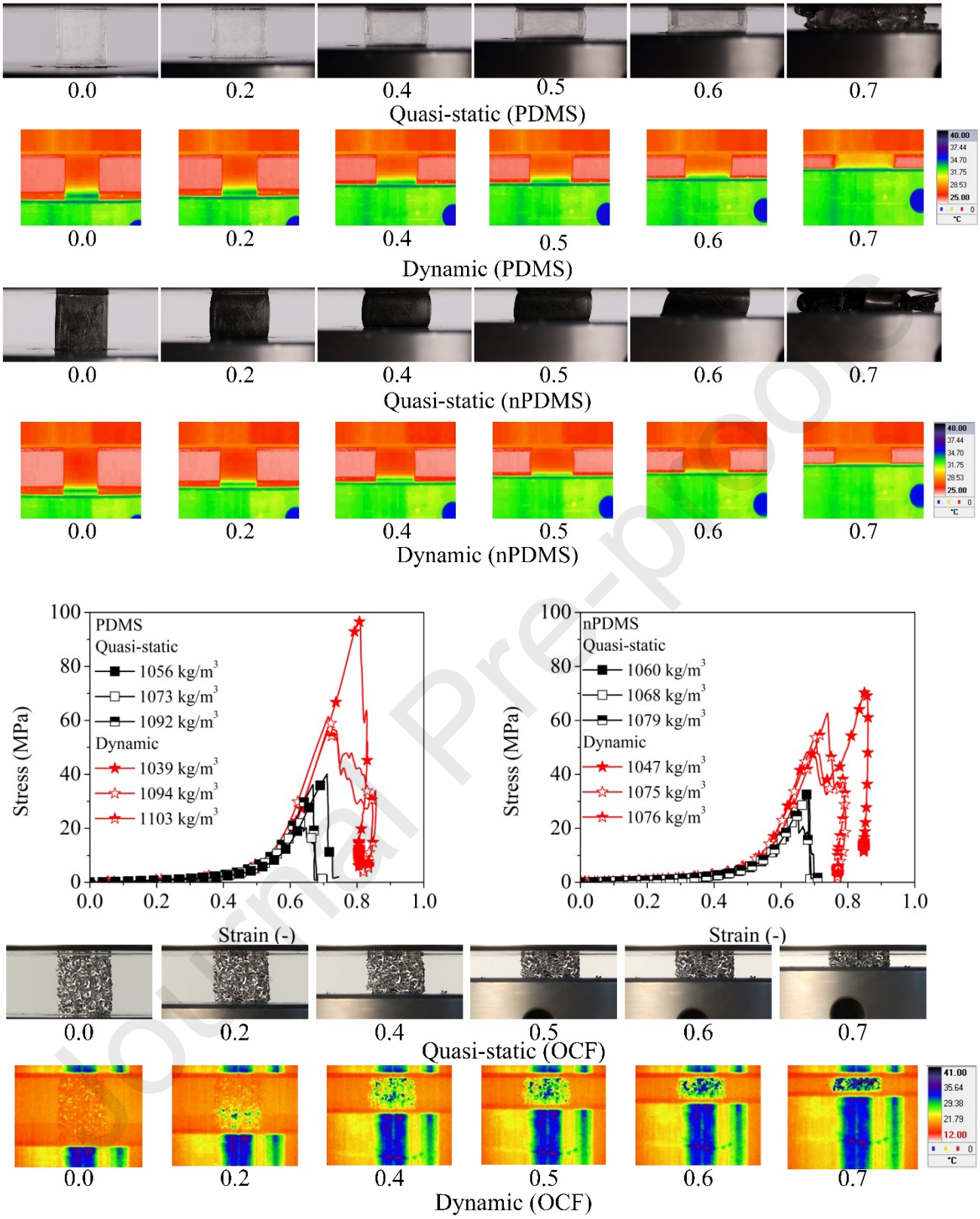

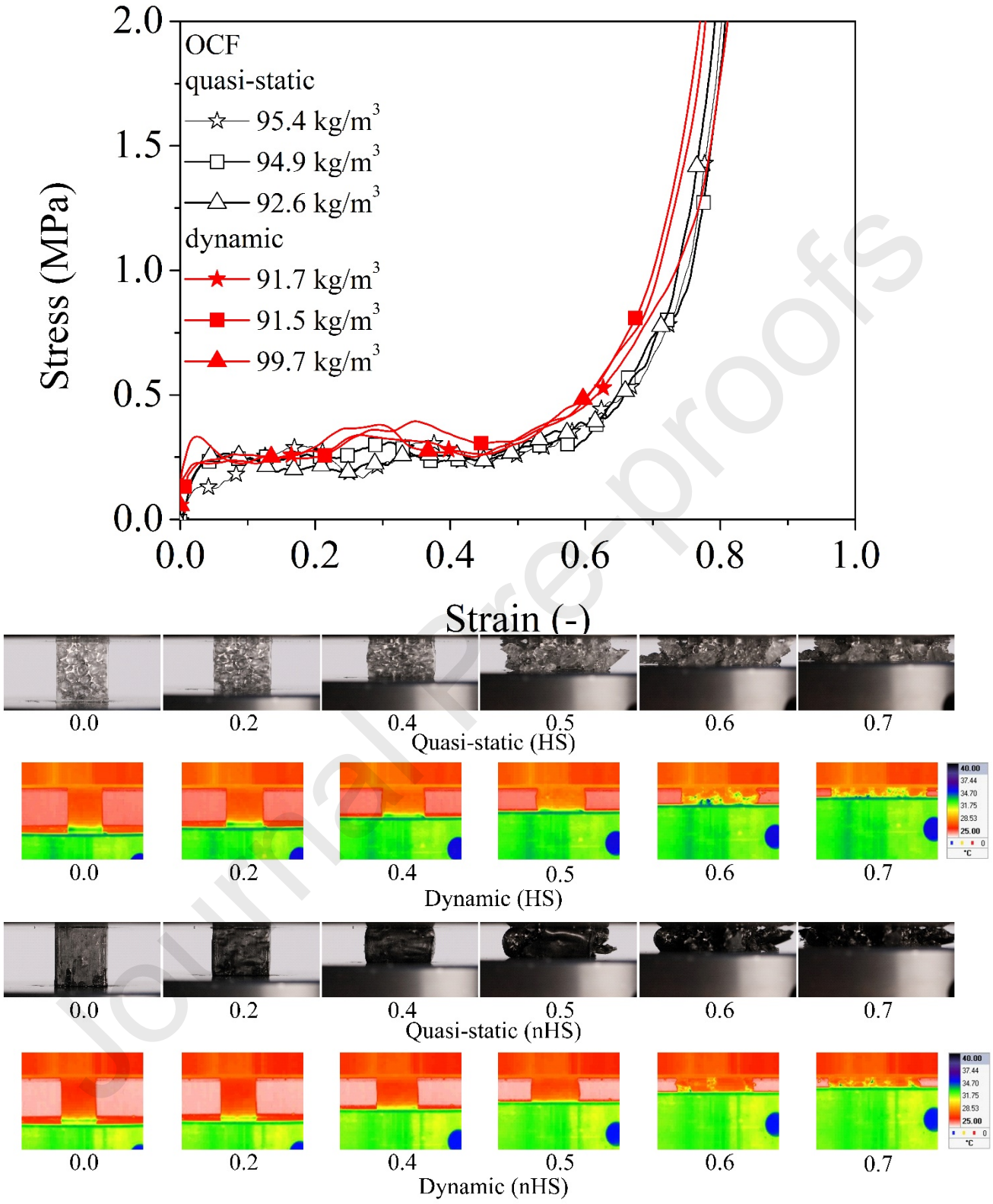

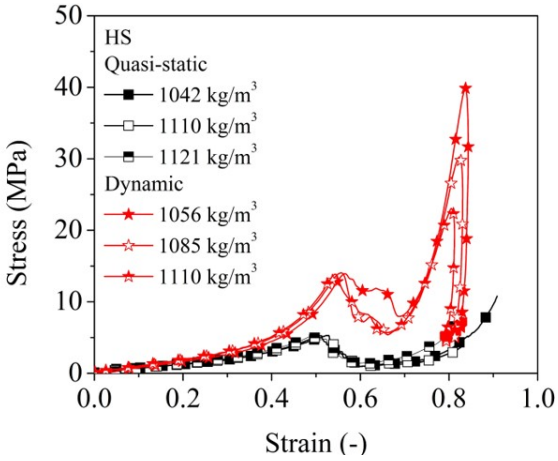

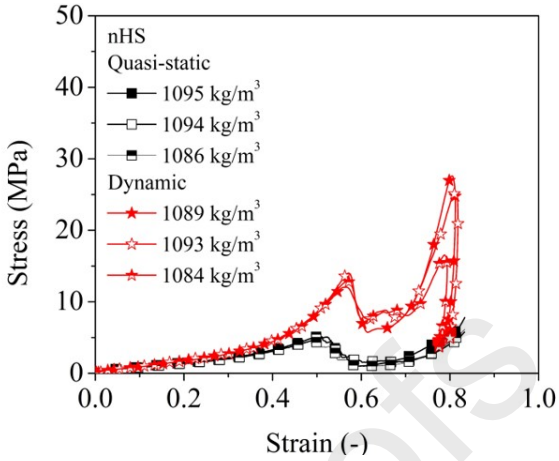

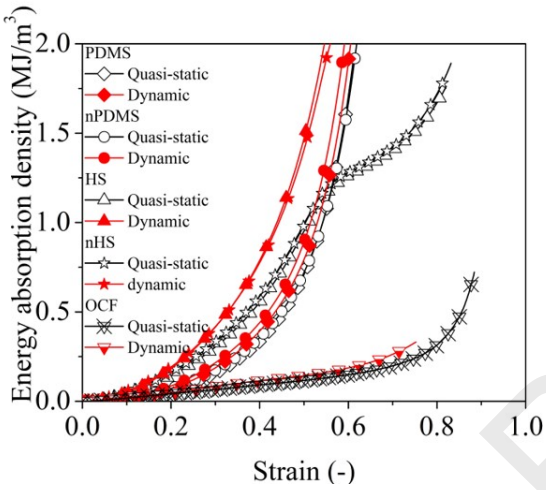

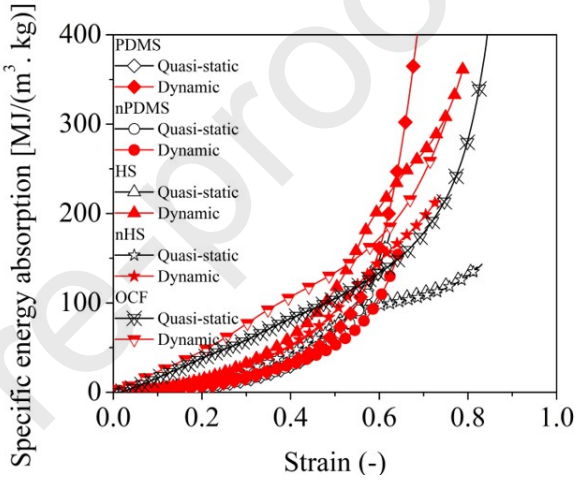

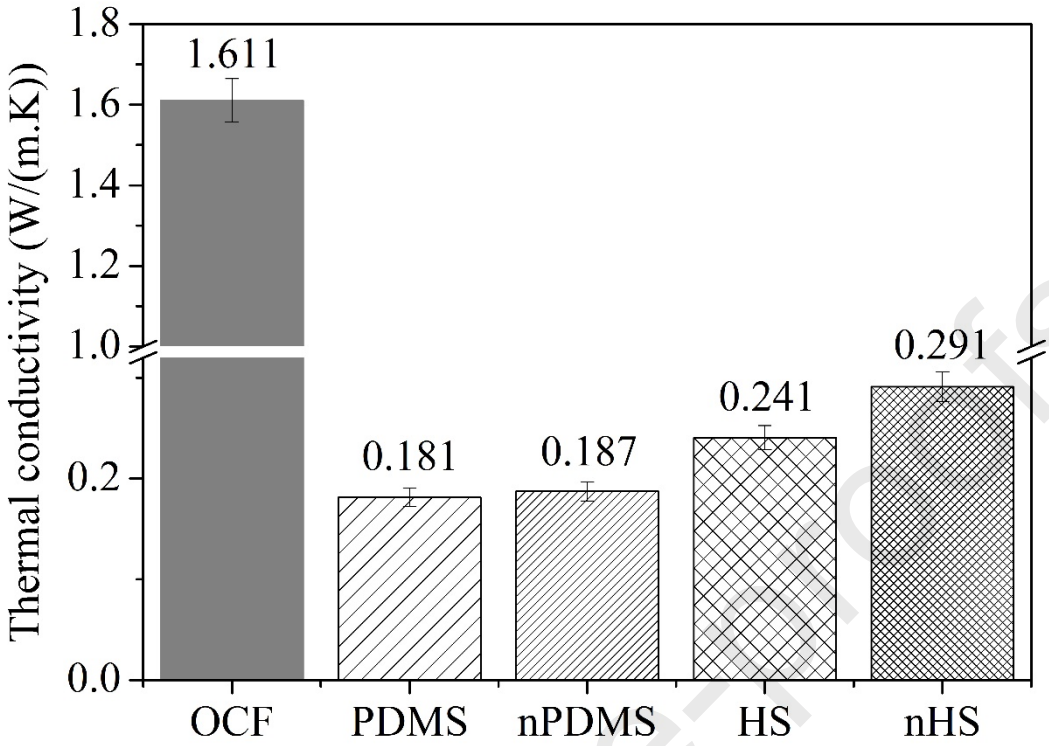

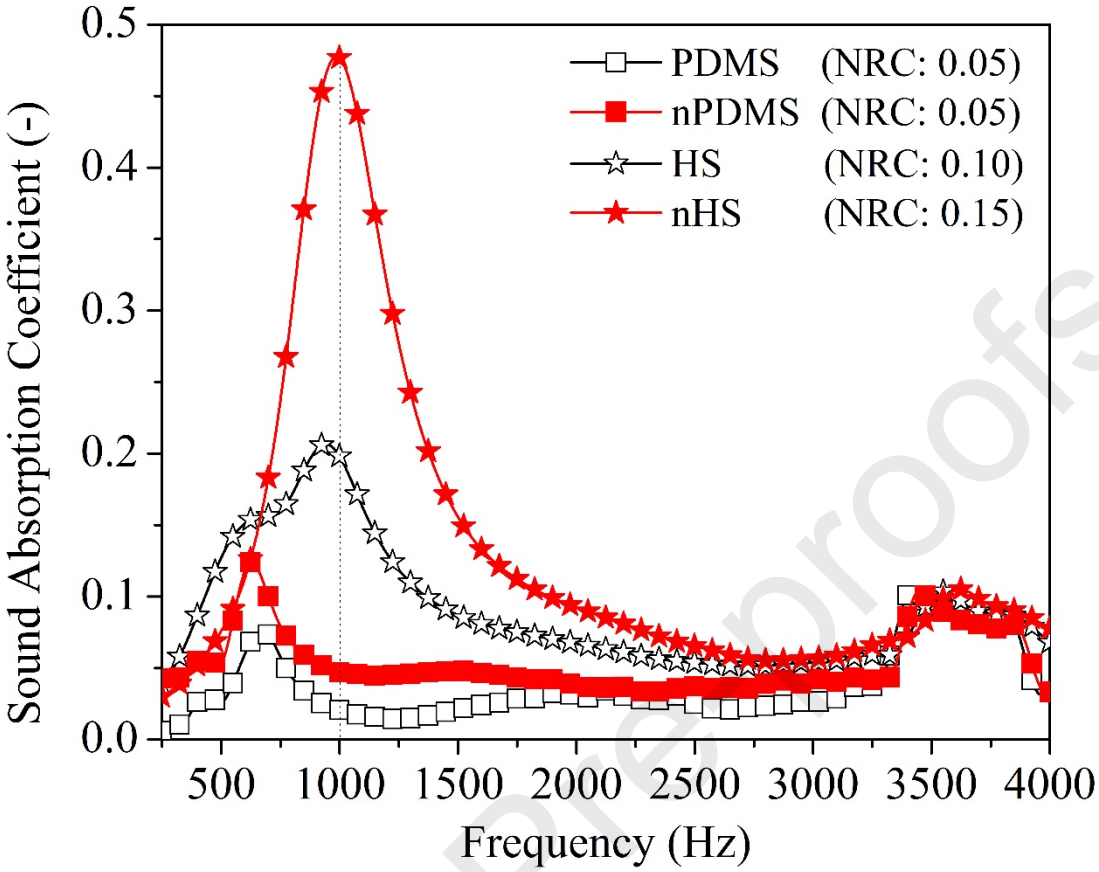

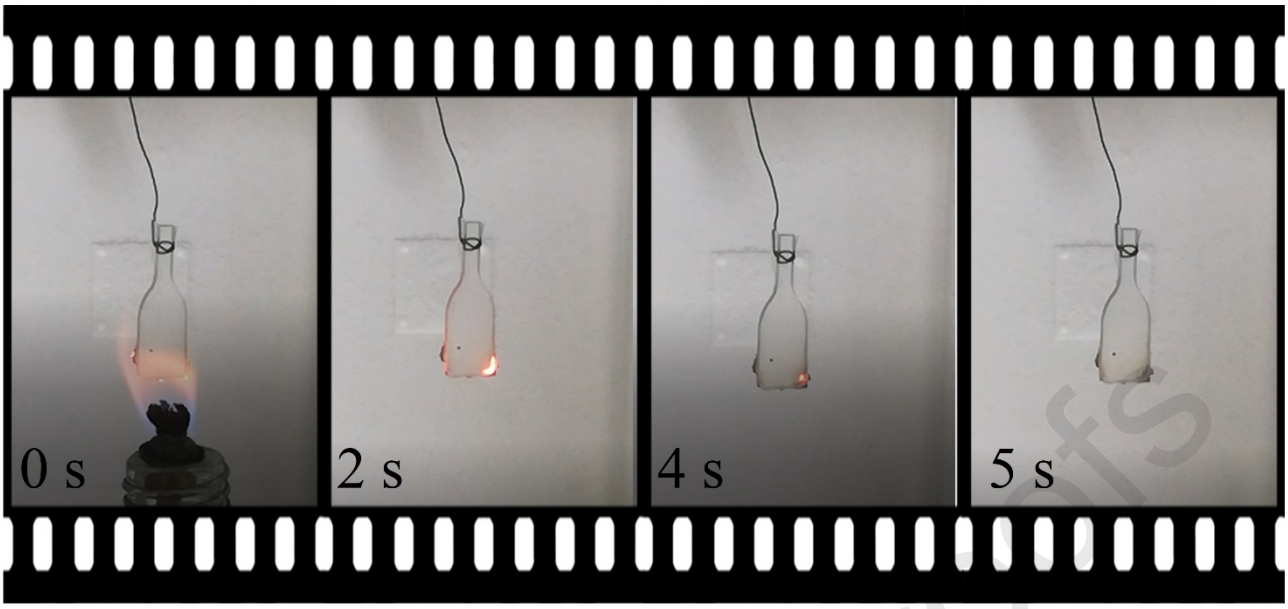

PDMS

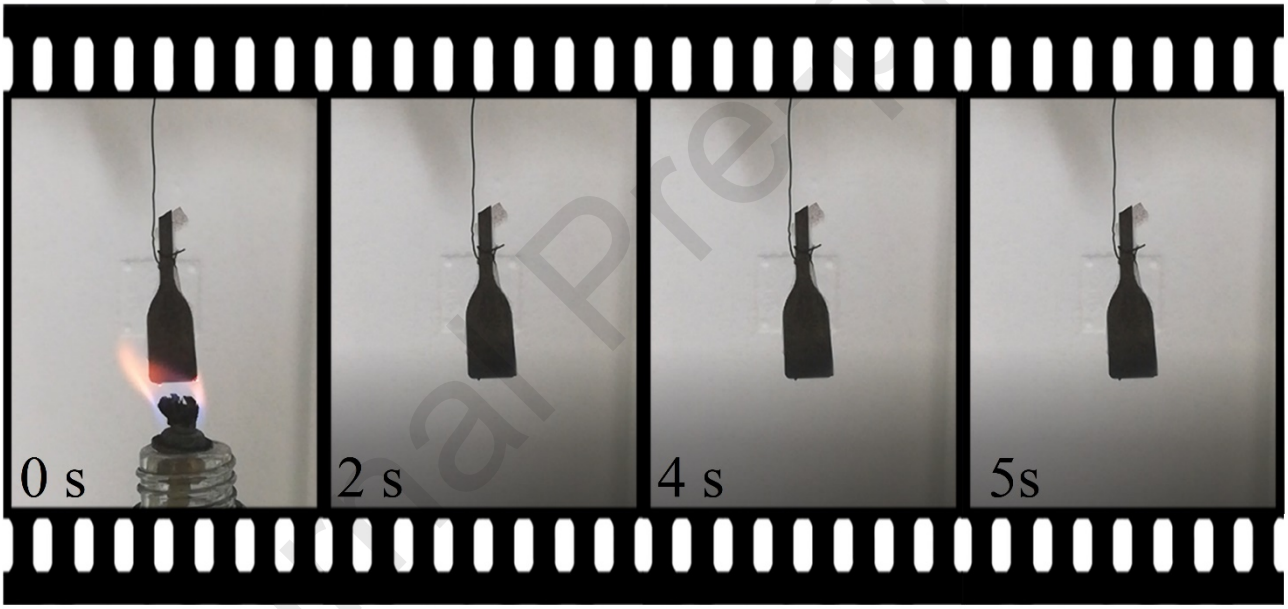

nPDMS

Table 1. Compressive results of PDMS and nPDMS specimens.

Specimen	Loading conditions	Density (kg/m^3)	Peak		Decay	
			Strain	Stress (MPa)	Strain	Stress (MPa)
		PDMS				
1		1056	0.71	40.11	0.73	1.58
2	Quasi-static	1073	0.62	22.44	0.68	1.12
3		1092	0.67	36.19	0.68	0.79
	Average	1074	0.67	32.91	0.70	1.16
	Standard deviation	18.0	0.044	9.28	0.029	0.39

1		1039	0.81	96.80		
2	Dynamic	1094	0.71	61.40	0.75	43.05
3		1103	0.71	56.06	0.75	39.82
	Average	1079	0.75	71.42	0.75	41.44
	Standard deviation	34.6	0.06	22.14	0.002	2.28
			nPDMS			
1		1060	0.68	33.26	0.70	1.16
2	Quasi-static	1068	0.68	32.25	0.69	1.14
3		1079	0.64	25.11	0.69	1.37
	Average	1069	0.67	30.21	0.70	1.22
	Standard deviation	9.5	0.02	4.44	0.006	0.125
1		1047	0.69	47.94	0.72	35.85
2	Dynamic	1075	0.70	54.12	0.74	32.49
3		1076	0.74	62.71	0.76	35.59
	Average	1066	0.71	54.92	0.74	34.64
	Standard deviation	16.5	0.03	7.42	0.02	1.87

Table 2. Compressive results of HFs and nHFs specimens.

Specimen	Loading conditions	Density (kg/m3)	First Peak		Decay	
			Strain	Stress (MPa)	Strain	Stress (MPa)
			HFs			
1		1042	0.51	5.25	0.60	0.95
2	Static	1110	0.53	5.31	0.60	0.95
3		1112	0.49	5.19	0.62	1.38
	Average	1088	0.51	5.25	0.61	1.09
	Standard deviation	39.8	0.02	0.06	0.012	0.25
1		1056	0.57	13.92	0.61	11.46
2	Dynamic	1085	0.56	14.05	0.59	7.68
3		1100	0.55	13.85	0.60	8.40
	Average	1080	0.56	13.94	0.60	9.18
	Standard deviation	22.4	0.01	0.10	0.01	2.01
			nHFs			
1		1095	0.50	5.16	0.60	1.00
2	Quasi-static	1094	0.52	5.07	0.60	1.53
3		1086	0.49	4.57	0.61	0.96
	Average	1092	0.50	4.93	0.60	1.16
	Standard deviation	4.9	0.02	0.32	0.005	0.32

1		1089	0.57	12.04	0.61	5.73
2	Dynamic	1093	0.57	14.02	0.61	7.20
3		1084	0.57	12.83	0.62	7.57
	Average	1089	0.57	12.97	0.61	6.83
	Standard deviation	4.5	0.003	0.996	0.006	0.98

Declaration of interests

☒ The authors declare that they have no known competing financial interests or personal relationships that could have appeared to influence the work reported in this paper.

☐The authors declare the following financial interests/personal relationships which may be considered as potential competing interests: